

# Interconversion between two unrelated protein folds in the lymphotactin native state

Robbyn L. Tuinstra\*, Francis C. Peterson\*, Snjezana Kutlesa†, E. Sonay Elgin‡, Michael A. Kron†§, and Brian F. Volkman\*¶

Departments of \*Biochemistry and †Medicine and ‡Biotechnology and Bioengineering Center, Medical College of Wisconsin, Milwaukee, WI 53226; and ‡Department of Chemistry, Kimya Bölümü Mugla Üniversitesi, Mugla 48000, Turkey

Edited by S. Walter Englander, University of Pennsylvania School of Medicine, Philadelphia, PA, and approved February 1, 2008 (received for review October 6, 2007)

Proteins often have multiple functional states, which might not always be accommodated by a single fold. Lymphotactin (Ltn) adopts two distinct structures in equilibrium, one corresponding to the canonical chemokine fold consisting of a monomeric three-stranded  $\beta$ -sheet and carboxyl-terminal helix. The second Ltn structure solved by NMR reveals a dimeric all- $\beta$ -sheet arrangement with no similarity to other known proteins. In physiological solution conditions, both structures are significantly populated and interconvert rapidly. Interconversion replaces long-range interactions that stabilize the chemokine fold with an entirely new set of tertiary and quaternary contacts. The chemokine-like Ltn conformation is a functional XCR1 agonist, but fails to bind heparin. In contrast, the alternative structure binds glycosaminoglycans with high affinity but fails to activate XCR1. Because each structural species displays only one of the two functional properties essential for activity *in vivo*, the conformational equilibrium is likely to be essential for the biological activity of lymphotactin. These results demonstrate that the functional repertoire and regulation of a single naturally occurring amino acid sequence can be expanded by access to a set of highly dissimilar native-state structures.

chemokine | conformational change | NMR spectroscopy

Protein folding converts 1D information encoded by a gene sequence into a biologically active 3D structure. Anfinsen's hypothesis (1) continues to inform our basic understanding of protein folding: a polypeptide achieves its biologically active, native state by descending to the most thermodynamically stable configuration, which corresponds to one of a few thousand unique folds (2). Although the existence of sequences that can adopt multiple unrelated folded states has been postulated (3), naturally occurring proteins exhibiting such native-state behavior have yet to be identified. Among proteins that fold spontaneously, the intrinsic dynamics typically include local fluctuations involving flexible loops or active-site residues, or concerted motions of entire subdomains. Large-scale rearrangements might involve partial unfolding or changes in oligomeric state, but even the most dramatic examples of reversible conformational change can be described as a perturbation on the native structure. For example, Arc repressor was engineered to permit exchange between the native structure and an alternative  $\alpha$ -helical "switch Arc" that are related by a localized  $\beta$ -sheet to  $\alpha$ -helix transformation (3). Likewise, slow interconversion of a monomeric mutant of the spindle checkpoint protein Mad2 repositions a C-terminal  $\beta$ -hairpin on an invariant core structure to allow Cdc20 binding, and at equilibrium  $\approx 10\%$  of the protein can be detected in the inactive state by NMR (4). In each case, the different conformations are closely related and share a majority of their stabilizing interactions (secondary structure and hydrophobic packing interactions) in common.

Thus, as new examples of conformational change have been described, the paradigm which emerged from Anfinsen's thermodynamic hypothesis has remained intact: each amino acid sequence maps to a single tertiary fold with varying amounts of local flexibility. However, we have identified a naturally occur-

ring protein that breaks the "one sequence, one fold" paradigm. The human chemokine lymphotactin (Ltn) exists in an unusual equilibrium between two conformations that at physiological conditions (37°C, 150 mM NaCl) are equally populated. The dual Ltn structures interconvert slowly on the NMR chemical-shift time scale and can be characterized separately by changing the temperature and ionic strength to shift the equilibrium from one species to the other (5).

Chemokines are small, secreted proteins that induce chemotaxis by adhering to cell-surface glycosaminoglycans on vascular endothelium and stimulating specific G protein-coupled receptors (GPCRs) expressed on target leukocytes (6). Approximately 50 chemokines have been identified and classified into four subfamilies based on the position of the conserved cysteines at the N terminus (7). Ltn is the sole member of the C family and lacks one of the two disulfide bonds present in all other chemokines (8). Comparison of the dual Ltn conformations demonstrates that a single polypeptide sequence can fold into two highly dissimilar native-state structures. One conformation binds glycosaminoglycans, whereas the other activates the Ltn receptor XCR1, but neither can perform both functions. Thus, this novel folding behavior has evolved for a biological purpose, perhaps to create a novel mechanism for strict regulation of T cell recruitment based on protein refolding.

## Results

The molecular structures of several chemokines have been determined (9), revealing a common tertiary fold that forms two types of dimeric structures (Fig. 1A). Under certain solution conditions (10°C, 200 mM NaCl), Ltn adopts the conserved chemokine fold, which we termed Ltn10 (10). However, NMR spectra at 25–37°C contain additional signals that correspond to a second conformation, and at higher temperature in the absence of salt, the Ltn10 spectrum is no longer visible (Fig. 1B). Each of the two conformations detected by NMR displays the chemical-shift dispersion typical of a stable, folded protein, but their resonance assignments and secondary structure patterns are entirely distinct, suggesting that a large-scale structural change occurs (5). Although Ltn10 is monomeric, the low-salt/high-temperature form self-associates with an affinity in the micromolar range (5), and the two species interconvert on a time

Author contributions: F.C.P., M.A.K., and B.F.V. designed research; R.L.T., F.C.P., S.K., E.S.E., and B.F.V. performed research; R.L.T. and F.C.P. contributed new reagents/analytic tools; R.L.T., F.C.P., S.K., E.S.E., and B.F.V. analyzed data; and R.L.T., F.C.P., and B.F.V. wrote the paper.

The authors declare no conflict of interest.

This article is a PNAS Direct Submission.

Data deposition: Atomic coordinates and chemical shift assignments for Ltn40 have been deposited in the Protein Data Bank, [www.pdb.org](http://www.pdb.org) (PDB ID code 2JP1) and the BioMagRes-Bank, [www.bmrb.wisc.edu](http://www.bmrb.wisc.edu) (accession no. 15215).

¶To whom correspondence should be addressed. E-mail: [bvolkman@mcw.edu](mailto:bvolkman@mcw.edu).

This article contains supporting information online at [www.pnas.org/cgi/content/full/0709518105/DCSupplemental](http://www.pnas.org/cgi/content/full/0709518105/DCSupplemental).

© 2008 by The National Academy of Sciences of the USA

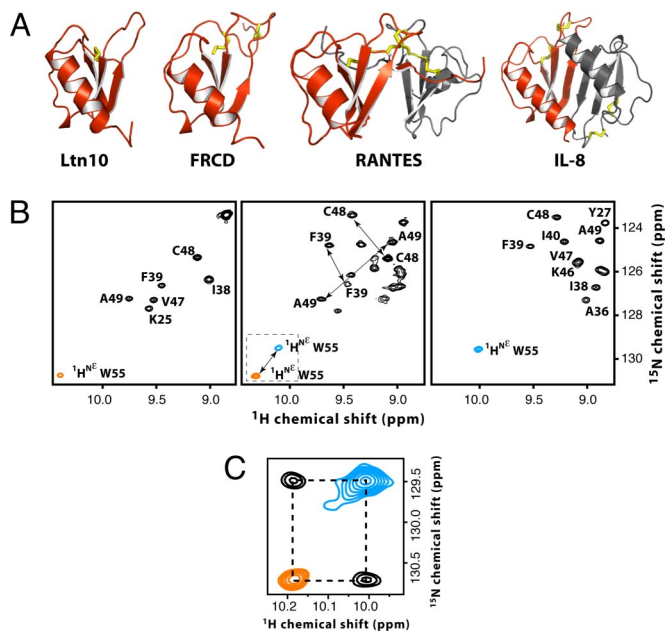


**Fig. 1.** Human Ltn exists in a two-state conformational equilibrium. (A) Members of the C (Ltn10), CX3C (fractalkine), CC (RANTES), and CXC (IL-8) chemokine families display a conserved tertiary structure. Distinct modes of dimerization are observed for the CC and CXC chemokines. (B) <sup>1</sup>H-<sup>15</sup>N HSQC spectra of Ltn at 10°C, 200 mM NaCl (Left) and 37°C, 150 mM NaCl (11) (Center), and 40°C, 0 mM NaCl (Right). Ltn exchanges slowly on the NMR chemical shift time scale between the Ltn10 and Ltn40 conformations, which are equally populated at near-physiological solution conditions. Arrows connect resonances for the same residue in the two conformational states. (C) Exchange peaks between the Ltn10 and Ltn40 <sup>1</sup>H-<sup>15</sup>N<sup>ε1</sup> resonances of Trp<sup>55</sup> in a 2D <sup>15</sup>N z-z-exchange spectrum (39), acquired with a 0.4-s mixing period.

scale of  $\approx 100$  ms (Fig. 1C). To compare their unique structural characteristics, we solved the structure of the WT Ltn dimer at 40°C.

At 40°C in the absence of salt, the second conformation (Ltn40) predominates, enabling us to determine the structure by standard NMR methods using NOE-derived distance constraints. We measured intermolecular NOEs by using an isotope-filtered NOESY experiment conducted on a mixture of <sup>15</sup>N/<sup>13</sup>C-labeled and unlabeled WT Ltn protein [supporting information (SI) Fig. S1]. Ltn40 adopts a novel four-stranded antiparallel  $\beta$ -sheet that self-associates as a head-to-tail dimer (Fig. 2A), with no apparent similarity to known structures (based on VAST and FATCAT queries). Positively charged side chains dominate the Ltn40 surface, but the dimer interface is composed of a central hydrophobic core and a cluster of charged residues at either end (Fig. 2B). Electrostatic stabilization of the dimer by the intermolecular Lys<sup>25</sup>-Glu<sup>31</sup> salt bridge (Fig. 2C) would be diminished in solutions of increasing ionic strength, which favor the Ltn10 conformation.

Structural changes associated with conversion from Ltn10 to Ltn40 are readily apparent (Fig. 3A), particularly the loss of  $\alpha$ -helical structure for residues 54–68 and formation of a new  $\beta$ -strand ( $\beta_0$ ) composed of residues 11–14 (5). This refolding process alters nearly all of the long-range contacts between residues. For example, Val<sup>15</sup> and Ala<sup>49</sup> pack together in the Ltn10 hydrophobic core but are separated by 18 Å in Ltn40. Likewise, new tertiary contacts in Ltn40 involve residue pairs (e.g., Leu<sup>14</sup> and Leu<sup>45</sup>) that were distant in Ltn10. As an objective measure of structural similarity, the contact matrix and an analogous plot of long-range NOEs for each Ltn structure (Fig. 3B) show that, except for the disulfide connecting Cys<sup>11</sup> and

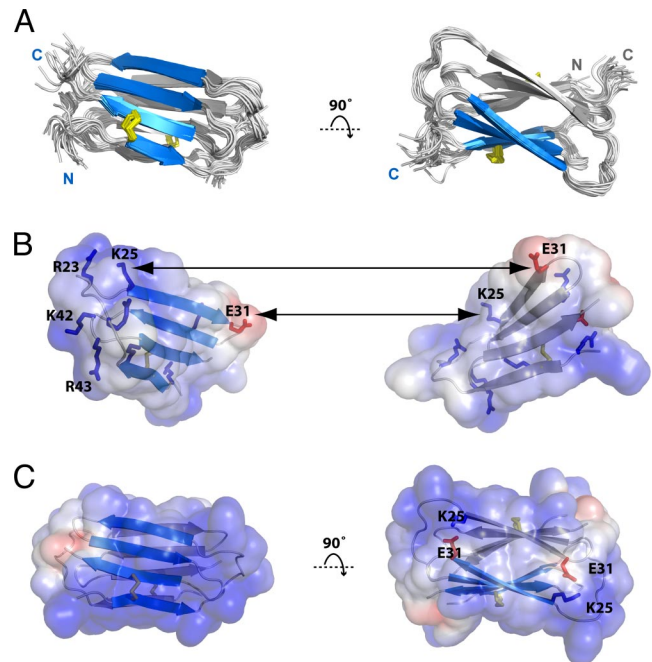


**Fig. 2.** Structure of the Ltn40 dimer. (A) Ensemble of 20 NMR structures with backbone rmsd  $\approx 0.5$  Å. Disordered N- and C-terminal residues (residues 1–7 and 53–93) are not shown. (B) Hydrophobic and electrostatic stabilization of the Ltn40 dimer. Lys<sup>25</sup> and a cluster of basic residues (blue) at one end of the dimer interface pair with Glu<sup>31</sup> and other acidic side chains (red) at the other end of the opposing monomer. Aliphatic and aromatic residues in the center (white surface) form the hydrophobic core of the dimer. (C) The electrostatic potential surface of the Ltn40 dimer is highly positive, owing to the large number of basic residues.

Cys<sup>48</sup>, virtually all Ltn10 tertiary interactions are replaced with different tertiary and quaternary contacts in Ltn40.

Except for a few residues in  $\beta_1$  and  $\beta_3$ , interconversion between the two structures repositions every side chain relative to the hydrophobic core, as if the protein was being turned inside out. Consequently, many residues show a dramatic reversal in solvent accessibility, as residues on the Ltn10 surface become part of the Ltn40 core and vice versa (Fig. 3C). For example, odd-numbered residues of the  $\beta_2$  strand that contribute to the Ltn10 hydrophobic core (Val<sup>37</sup>, Phe<sup>39</sup>, and Thr<sup>41</sup>) are instead displayed on the Ltn40 surface (Fig. 3D), whereas the even-numbered residues (Leu<sup>34</sup>, Ala<sup>36</sup>, Ile<sup>38</sup>, and Ile<sup>40</sup>) are reoriented from the Ltn10 surface to the hydrophobic interior of the Ltn40 dimer. Consequently, each structure is stabilized by an entirely different set of hydrophobic contacts.

This repositioning of hydrophobic contacts results from inversion of strands  $\beta_1$  and  $\beta_3$  and translation by one residue relative to the central  $\beta_2$  strand to assemble the Ltn40  $\beta$ -sheet. At the same time, residues 11–15 of the N-loop, which lay across the  $\beta$ -sheet and pack against the C-terminal helix in Ltn10, associate with newly exposed residues of  $\beta_3$  to form the new  $\beta_0$  strand. In the process, every hydrogen bond stabilizing the secondary structure of one conformation is broken and replaced with a new one involving a different pair of residues (Fig. 3E). For example, Val<sup>47</sup> ( $\beta_3$ ) pairs with Phe<sup>39</sup> ( $\beta_2$ ) in Ltn10 but with Val<sup>12</sup> ( $\beta_0$ ) in Ltn40. Hydrogen bonds lost in unfolding of the C-terminal  $\alpha$ -helix of Ltn10 are compensated in Ltn40 by additional  $\beta$ -sheet structure and hydrophobic packing at the dimer interface. Thus, the Ltn sequence interconverts between two folded native-state structures defined by mutually exclusive sets of stabilizing interactions.

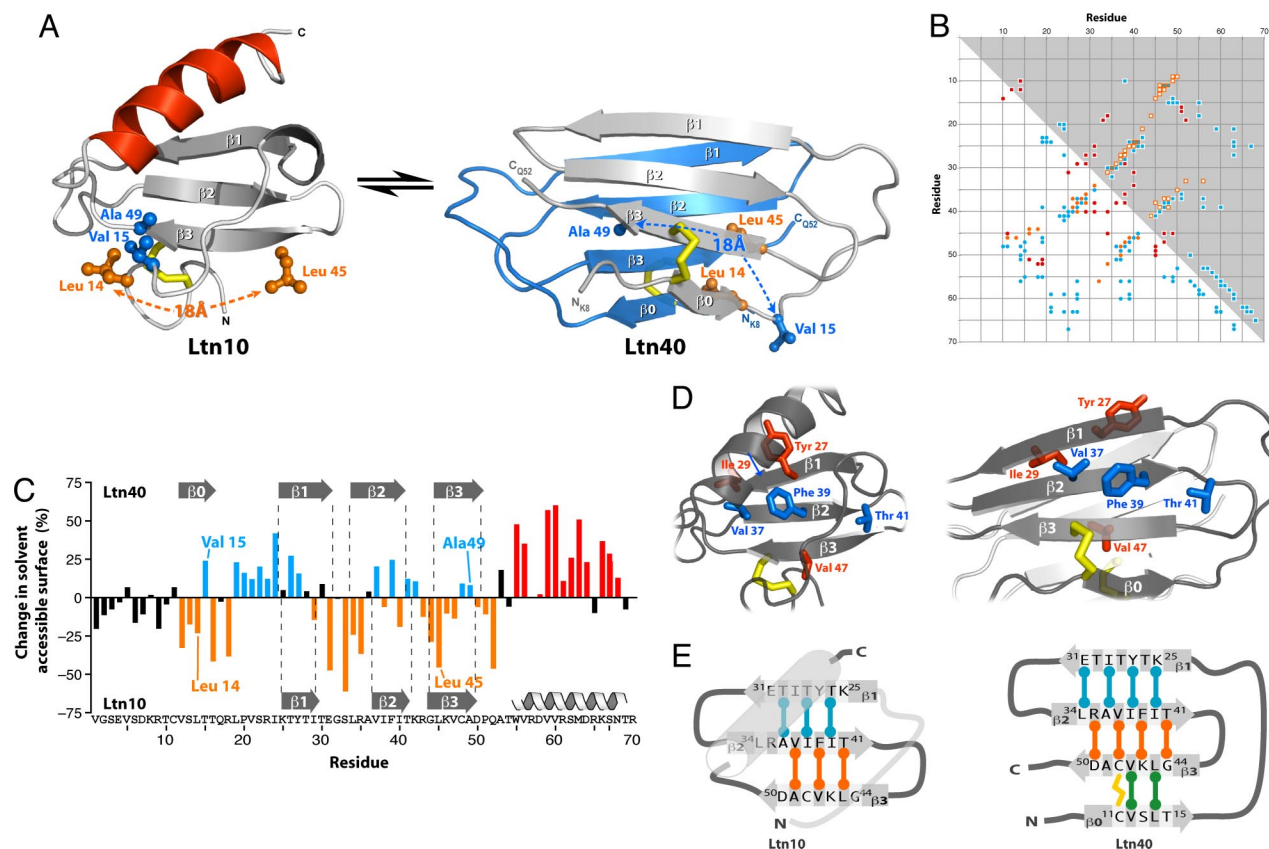


**Fig. 3.** Native Ltn exchanges between two unrelated structures. (A) Ltn10  $\leftrightarrow$  Ltn40 interconversion alters all tertiary contacts. Val<sup>15</sup> and Ala<sup>49</sup> pack together in the Ltn10 hydrophobic core (Left) but are separated by 18 Å in Ltn40 (Right), whereas the converse is true for Leu<sup>14</sup> and Leu<sup>45</sup>. (B) Ltn10 and Ltn40 exhibit markedly different patterns of long-range contacts. NOE distance constraints for Ltn10 (blue circles) and Ltn40 (orange circles, intramolecular; red circles, intermolecular) are plotted below the diagonal. Close contacts (<2.5 Å) observed in >80% of the NMR structure ensemble are plotted above the diagonal for residues of Ltn10 (blue squares) and Ltn40 (white squares, intramolecular; red squares, intermolecular). (C) Relative changes in solvent-accessible surface (SAS) calculated as  $SAS_{Ltn40} - SAS_{Ltn10}$ , expressed as the percentage of total surface area for each side chain. Highlighted residues are more solvent-exposed in either Ltn10 (cyan) or Ltn40 (orange). Residues on the Ltn10 surface (orange) reside in the core of the Ltn40 structure, whereas Ltn40 surface residues (cyan) are located in the Ltn10 interior. (D) (Left) The odd-numbered residues of  $\beta 1$  (orange),  $\beta 2$  (cyan), and  $\beta 3$  (orange) contribute to the Ltn10 core. (Right) In the Ltn40 native-state conformer, the odd-numbered side chains of  $\beta 1$  and  $\beta 3$  pack in the dimer interface, whereas the odd-numbered residues of  $\beta 2$  are reoriented to the opposite face of the  $\beta$ -sheet and reside on the surface. (E) Rearrangement of hydrogen bonds defining the Ltn secondary structure. Each bar denotes a pair of backbone N-H...O = C hydrogen bonds connecting  $\beta 1$ - $\beta 2$  (cyan),  $\beta 2$ - $\beta 3$  (orange), and  $\beta 0$ - $\beta 3$  (green). Ltn10  $\leftrightarrow$  Ltn40 interconversion shifts  $\beta 2$  by one residue relative to  $\beta 1$  and  $\beta 3$ , which rotate 180° and establish a new hydrogen bond pattern with residues of  $\beta 0$  and  $\beta 2$ .

Why would nature select for a protein sequence that adopts two unrelated structures? Like many proteins, chemokines must interact with multiple binding partners to perform their biological functions *in vivo*. Binding to extracellular matrix glycosaminoglycans facilitates cell surface retention and chemokine gradient formation (11, 12). GPCR activation on a target leukocyte stimulates extravasation from the bloodstream and migration toward the chemokine source (13, 14). We hypothesized that Ltn10 and Ltn40 each might participate in Ltn biology and that their interconversion provides a novel mechanism for switching between two functional states.

Because the Ltn10–Ltn40 equilibrium is near its midpoint in physiological solution conditions ( $K_{eq} \approx 1$  at 37°C, 150 mM NaCl), it is difficult to measure the biological activity of each species independently. Consequently, we produced Ltn variants designed to eliminate the conformational equilibrium and adopt only the Ltn10 (CC3) or Ltn40 (W55D) structure (Fig. 4A). The additional disulfide cross-link in CC3 preserves the Ltn10 structure and prevents conversion to Ltn40 (15). Conversely, substitution of aspartic acid for Trp<sup>55</sup>, a central element in the Ltn10 hydrophobic core, shifts the conformational equilibrium by increasing the relative stability of Ltn40. 2D NMR shows that

W55D adopts the Ltn40 structure with no evidence of interconversion to the Ltn10 conformation (Fig. 4A).

We first compared WT Ltn, CC3, and W55D in their ability to activate the XCR1 receptor (Fig. 4B). Chemokine-mediated activation of the cognate GPCR elicits signal transduction events and influx of intracellular  $Ca^{2+}$ , and we monitored the response of XCR1-expressing cells to each protein. In contrast to WT Ltn and CC3 (15), W55D is not functional as an XCR1 agonist at all concentrations tested (50–750 nM). We also measured the migratory response of primary human CD3<sup>+</sup> T cells to each Ltn protein. Wild-type Ltn and CC3 induced maximal chemotactic migration at protein concentrations of 1–10 nM, but W55D produced no detectable chemotaxis at 0.1–100 nM (data not shown).

Like other chemokines (16), Ltn binds heparin with high affinity, and its *in vivo* activity depends on GAG interactions (17). Wild-type Ltn elutes from a heparin-Sepharose column in two distinct fractions (Fig. 4C), suggesting that the Ltn10 and Ltn40 species bind with different affinities. The CC3 and W55D proteins elute at salt concentrations that match the low- and high-affinity fractions, respectively, suggesting that Ltn40 binds glycosaminoglycans more strongly than Ltn10 does.

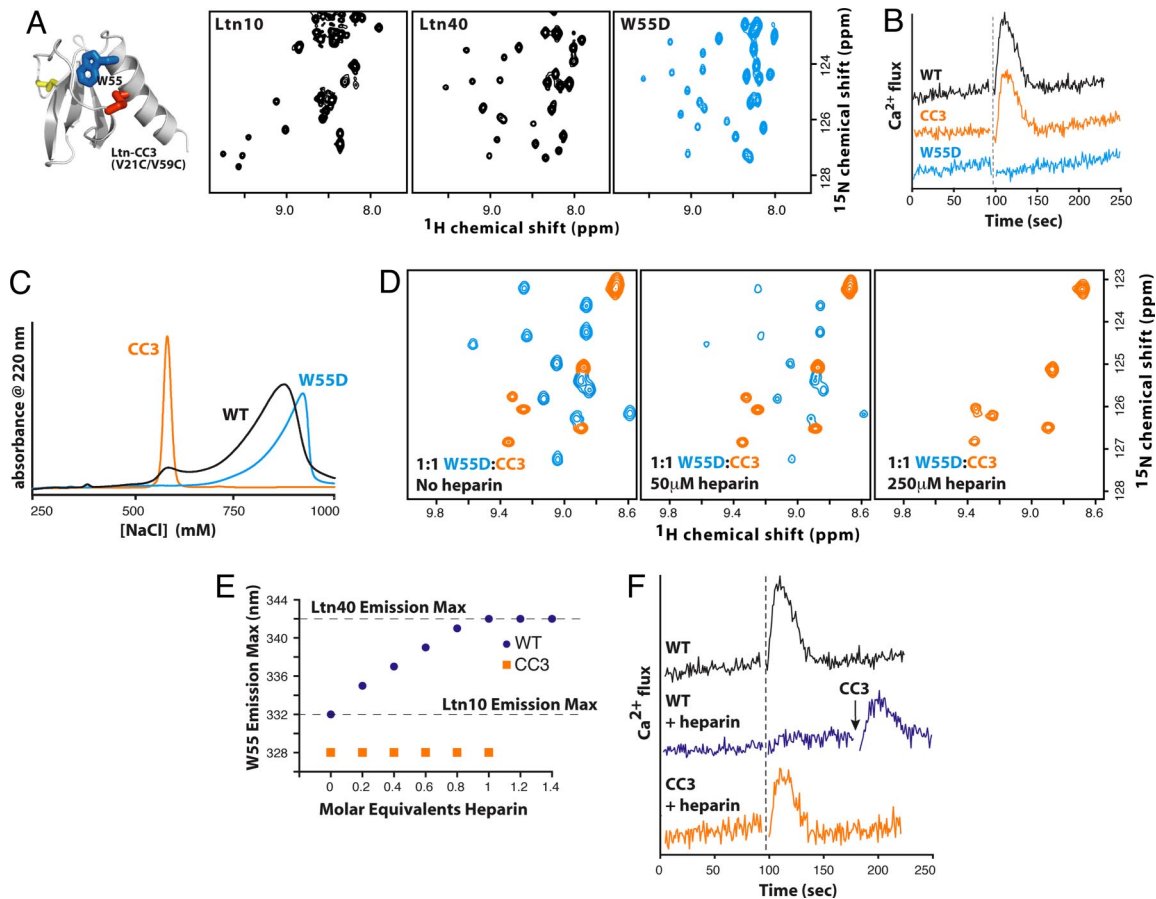


**Fig. 4.** Ltn10 and Ltn40 are functionally distinct. (A) An engineered disulfide (red) locks the CC3 variant into the Ltn10 fold (15), but replacement of Trp<sup>55</sup> (blue) with Asp (W55D) yields exclusively the Ltn40 species. With the exception of signals adjacent to the amino acid substitution, the HSQC spectrum of W55D is identical to the Ltn40 spectrum obtained with WT Ltn. (B) Ca<sup>2+</sup> flux response of XCR1 expressing HEK293 cells to WT (black), CC3 (orange), and W55D (blue) Ltn. Dashed line marks the addition of 200 nM chemokine. (C) Elution profiles for WT (black), CC3 (orange), and W55D (blue) Ltn from heparin-Sepharose. (D) Heparin selectively precipitates the Ltn40 conformation. (Left) Before the addition of heparin tetrasaccharide, HSCF signals are observed for both W55D (blue) and CC3 (orange). (Center and Right) Heparin addition results in the broadening (Center) and disappearance of W55D amide peaks (Right). (E) Titration of WT Ltn with semipurified heparin shifts the conformational equilibrium toward Ltn40 based on changes in the Trp<sup>55</sup> emission wavelength (blue). CC3 emission is unaltered by heparin (orange). Emission maxima for Ltn10 and Ltn40 are indicated. (F) Ca<sup>2+</sup> flux response of WT (black) and CC3 (orange) after incubation with an equimolar concentration of semipurified heparin. Heparin prevents WT Ltn-XCR1 association, as sequential addition of CC3 elicits XCR1 activation.

To test this hypothesis, an equimolar mixture of [*U*-<sup>15</sup>N]W55D and [*U*-<sup>15</sup>N]CC3 was titrated with purified heparin tetrasaccharide and the interaction was followed by NMR spectroscopy (Fig. 4D). Association with GAGs has been shown to facilitate chemokine oligomerization (16), often resulting in insoluble protein–heparin complexes (18). When both Ltn conformations are present in solution, heparin binds only to the Ltn40 structure (Fig. 4D). This is evident from the loss of W55D signals caused by precipitation of W55D–heparin complexes, whereas CC3 remained in solution with no perturbation in amide chemical shifts.

Based on these results, we examined the hypothesis that conformation-specific GAG binding would shift the Ltn structural equilibrium and modulate its activity. We first monitored the intrinsic fluorescence emission of Trp<sup>55</sup>, which shifts to longer wavelengths (red shift) upon the transition from a buried, hydrophobic environment (Ltn10) to a flexible, solvent-exposed state (Ltn40) (5). Titration of WT Ltn with low molecular weight heparin induces a red shift in the fluorescence spectrum corresponding to the conversion of Ltn10 to Ltn40, whereas the CC3 protein is unaffected (Fig. 4E). Disruption of Ltn-heparin binding by the addition of 1 M NaCl restores the Ltn10 fluorescence spectrum. Strikingly, heparin prevents Ltn activation of XCR1

by WT Ltn, but not CC3 (Fig. 4F), presumably by preventing interconversion and suppressing the agonist activity associated with the Ltn10 species. These results show that the Ltn conformational equilibrium can be influenced by interactions with its binding partners.

## Discussion

The theoretical basis for protein folding remains a topic of active debate, even on issues as fundamental as whether the backbone or side chains provide the driving force for folding (19). Nevertheless, experimental structural biology continues to support the notion that proteins spontaneously adopt one of a few thousand unique folds. Although Ltn may be the first naturally occurring protein found to interconvert between unrelated native-state structures, “evolutionary bridges” connecting two distinct folds have been predicted (3), and this phenomenon likely occurs elsewhere in the protein structure universe. As with the analysis of intrinsically unfolded proteins (20, 21), dynamic structural heterogeneity has typically been detected by solution NMR methods (22–24). It may be that crystallization is generally incompatible with proteins that exhibit multiple states related by large differences in conformation and that most structural biology efforts have inadvertently selected against their detection.

To underscore the biological relevance of Ltn structural interconversion, we showed that the Ltn10 and Ltn40 structures are functionally complementary, because each one encodes an essential interaction that combines to induce cell migration *in vivo*. Without the chemokine-like Ltn10 conformation, Ltn cannot bind and activate the XCR1 receptor on the surface of a target cell. Conversely, only the novel Ltn40 state provides high-affinity binding to extracellular matrix glycosaminoglycans to maintain a chemotactic concentration gradient. At the same time, GAG binding inhibits Ltn activity by sequestering the protein in the Ltn40 state. Ltn has thus evolved a novel mechanism for regulating biological activity by switching between two structures that display distinct binding surfaces on completely unrelated protein folds.

Ltn molecules bound to the extracellular matrix as Ltn40 must dissociate and switch to the Ltn10 structure to stimulate XCR1 on a circulating T cell. However, we lack a mechanistic understanding of conversion from the inactive, GAG-bound Ltn40 state to the active Ltn10 species in a functional context. The same question applies to chemokines generally, most of which self-associate in the presence of GAGs. Is chemokine mobilization an active process, driven by enzymes that degrade the extracellular matrix, or is it governed simply by changes in local concentration that shift binding and conformational equilibria? As with other GAG-bound chemokine oligomers, the details of this protein structure transition at the interface between vascular endothelium and circulating leukocytes require further investigation.

## Methods

**Protein Expression, Purification, and Mutagenesis.** Recombinant human Ltn for structural studies was expressed and purified as described (17), yielding a protein that lacks the N-terminal Val residue corresponding to Ltn(2–93). Cyanogen bromide cleavage was used to generate an Ltn(1–93) protein with the native N-terminal sequence that also contains the amino acid substitutions M63A and M72A (15). Ltn(M63V/M72A) behaved identically to WT recombinant Ltn(1–93) protein produced by another method (10) in 2D NMR and  $\text{Ca}^{2+}$ -flux measurements, demonstrating that Ltn structure and activity are unaltered by the two methionine substitutions (15). Purity, identity, and molecular weight were verified by MALDI-MS and NMR. Site-directed mutagenesis was performed by using pairs of complementary primers and the QuikChange kit (Stratagene). All expression vectors were verified by DNA sequencing. Purified Ltn was frozen, lyophilized, and stored at  $-20^{\circ}\text{C}$ .

**In Vitro Calcium Flux Assay for XCR1 Activation.** XCR1 activation was monitored by the increase in intracellular  $\text{Ca}^{2+}$  as described (15) using HEK 293 cells stably expressing XCR1 (25). All data have been normalized to carbachol control.

**Chemotaxis Assay.** Primary human lymphocytes were isolated from healthy donor buffy coat within 24–48 h under an institutional review board-approved protocol by Ficoll gradient followed by MACS separation with CD3 MicroBeads (Miltenyi Biotech).  $\text{CD}3^{+}$  T cells were resuspended at  $1\text{--}5 \times 10^6$  cells/ml in RPMI medium 1640 enriched with 1% BSA, 25 mM HEPES, pH 8.0. Chemotaxis assays were conducted in triplicate for each protein in a 48-well Neuroprobe Boyden chamber using 5- $\mu\text{m}$  polycarbonate membranes pre-coated with 50  $\mu\text{g}/\text{ml}$  of fibronectin (BD Bioscience) at  $37^{\circ}\text{C}$  for 2 h. Wild-type,

CC3, and W55D Ltn proteins were diluted in binding media and placed in the lower wells of a chemotaxis chamber, and 50  $\mu\text{l}$  of lymphocyte suspension was placed in the upper wells. The filled chemotaxis chambers were incubated in a humidified  $\text{CO}_2$  incubator for 3 h. After incubation membranes were removed from the chemotaxis chamber assembly. The cells from the upper side of the membrane were gently removed by rinsing in PBS solution, and the cells from the lower side of the membrane were fixed and stained with Rapid Stain (Richard-Allen Scientific). Cells that migrated across the membrane were counted under a microscope at  $\times 200$  magnification.

**Heparin Binding Experiments and Fluorescence Spectroscopy.** Semipurified heparin (average molecular mass of 3,000 Da) was purchased from Sigma. Purified heparin tetrasaccharide was obtained from R. L. Linhardt (Rensselaer Polytechnic Institute, Troy, NY). Ltn fluorescence experiments were conducted with an excitation wavelength of 285 nm by using a PTI fluorimeter with Peltier temperature control.

**NMR Spectroscopy.** NMR experiments were performed on a Bruker DRX 600 equipped with a  $^1\text{H}/^{15}\text{N}/^{13}\text{C}$  Cyroprobe. NMR samples contained 90%  $\text{H}_2\text{O}$ , 10%  $\text{D}_2\text{O}$ , and 0.02%  $\text{NaN}_3$ , with 20 mM sodium phosphate at pH 6.0. Ltn contains no histidine, and its NMR spectra and structural equilibrium are insensitive to changes in pH ranging from 5 to 8. Temperature and NaCl concentration were varied as specified in figure legends. Complete  $^1\text{H}$ ,  $^{15}\text{N}$ , and  $^{13}\text{C}$  resonance assignments for Ltn40 (20 mM sodium phosphate, pH 6.0) were obtained at  $40^{\circ}\text{C}$  by using the following experiments:  $^{15}\text{N}$ - $^1\text{H}$  HSQC (26), 3D HNCA (27, 28), 3D HNCO (27, 29), 3D HN(CO)CA (27), 3D HNCACB, 3D HN(CA)CO, 3D HCONH, 3D SE C(CO)NH (30), 3D HCCH TOCSY (31), and 2D  $^{13}\text{C}$  constant time HSQC (32). NMR data were processed with NMRPipe (33), and XEASY (34) was used for resonance assignments and analysis of NOE spectra.

**Structure Calculation and Analysis.** A total of 131 backbone and dihedral angle constraints (for residues 10–51) were generated from secondary shifts of the  $^1\text{H}^{\alpha}$ ,  $^{13}\text{C}^{\alpha}$ ,  $^{13}\text{C}^{\beta}$ ,  $^{13}\text{C}^{\gamma}$ , and  $^{15}\text{N}$  nuclei shifts by using the program TALOS (35). A total of 1,320 unique, nontrivial NOE distance constraints were obtained from 3D  $^{15}\text{N}$ -edited NOESY-HSQC (36),  $^{13}\text{C}$ (aliphatic)-edited NOESY-HSQC (31) ( $\tau_{\text{mix}} = 80$  ms), and F1- $^{13}\text{C}/^{15}\text{N}$ -filtered/F3- $^{13}\text{C}$ -edited NOESY spectra ( $\tau_{\text{mix}} = 120$  ms). To discern intermonomer NOEs, an F1- $^{13}\text{C}/^{15}\text{N}$ -filtered/F3- $^{13}\text{C}$ -edited NOESY experiment was conducted by using a mixed sample containing 50%  $^{13}\text{C}/^{15}\text{N}$ -Ltn and 50% unlabeled Ltn. Using the filtered NOESY pulse scheme, a significant portion of intramonomer and intraresidue NOEs have been eliminated (Fig. S1). Preliminary analysis of the filtered NMR spectrum identified 34 intermolecular NOEs that were incorporated as distance constraints in a preliminary structure calculation using the CYANA 2.1 program. The resulting dimeric structure was then used as the reference structure in an automated NOE assignment (NOEASSIGN) routine in CYANA, which assigned an additional 47 intermonomer distance constraints and produced an ensemble with high precision and low residual constraint violations that required minimal additional refinement. The 20 CYANA conformers with the lowest target function were subjected to a molecular dynamics protocol in explicit solvent (37) by using X-PLOR-NIH (38). Completely disordered residues 61–93 were not included in water refinement calculations, thus the ensemble of Ltn40 NMR structures deposited in the Protein Data Bank contains only residues 1–60. NMR structure refinement statistics are provided in Table S1.

**ACKNOWLEDGMENTS.** We thank Tina Liu for assistance with fluorescence measurements. This work was supported by National Institutes of Health Grants R01 AI45843 and R01 AI063325 (to B.F.V.) and UO1 AI053877 (to M.A.K.).

- Anfinsen CB (1973) Principles that govern the folding of protein chains. *Science* 181:223–230.
- Chothia C (1992) Proteins: One thousand families for the molecular biologist. *Nature* 357:543–544.
- Cordes MH, Burton RE, Walsh NP, McKnight CJ, Sauer RT (2000) An evolutionary bridge to a new protein fold. *Nat Struct Biol* 7:1129–1132.
- Luo X, et al. (2004) The Mad2 spindle checkpoint protein has two distinct natively folded states. *Nat Struct Mol Biol* 11:338–345.
- Kuloglu ES, McCaslin DR, Markley JL, Volkman BF (2002) Structural rearrangement of human lymphotactin, a C chemokine, under physiological solution conditions. *J Biol Chem* 277:17863–17870.
- Rossi D, Zlotnik A (2000) The biology of chemokines and their receptors. *Annu Rev Immunol* 18:217–242.
- Zlotnik A, Yoshie O (2000) Chemokines: A new classification system and their role in immunity. *Immunity* 12:121–127.
- Kelner G, et al. (1994) Lymphotactin: A cytokine that represents a new class of chemokine. *Science* 266:1395–1399.
- Clark-Lewis I, et al. (1995) Structure-activity relationships of chemokines. *J Leukocyte Biol* 57:703–711.
- Kuloglu ES, et al. (2001) Monomeric solution structure of the prototypical C chemokine lymphotactin. *Biochemistry* 40:12486–12496.
- Middleton J, et al. (1997) Transcytosis and surface presentation of IL-8 by venular endothelial cells. *Cell* 91:385–395.
- Sweeney EA, Lortat-Jacob H, Priestley GV, Nakamoto B, Papayannopoulou T (2002) Sulfated polysaccharides increase plasma levels of SDF-1 in monkeys and mice: Involvement in mobilization of stem/progenitor cells. *Blood* 99:44–51.
- Campbell JJ, et al. (1998) Chemokines and the arrest of lymphocytes rolling under flow conditions. *Science* 279:381–384.
- Proudfoot AE, et al. (2003) Glycosaminoglycan binding and oligomerization are essential for the *in vivo* activity of certain chemokines. *Proc Natl Acad Sci USA* 100:1885–1890.
- Tuinstra RL, Peterson FC, Elgin ES, Pelzek AJ, Volkman BF (2007) An engineered second disulfide bond restricts lymphotactin/XCL1 to a chemokine-like conformation with XCR1 agonist activity. *Biochemistry* 46:2564–2573.

16. Hoogewerf AJ, et al. (1997) Glycosaminoglycans mediate cell surface oligomerization of chemokines. *Biochemistry* 36:13570–13578.
17. Peterson FC, et al. (2004) Identification and characterization of a glycosaminoglycan recognition element of the C chemokine lymphotactin. *J Biol Chem* 279:12598–12604.
18. Stura EA, Martin L, Lortat-Jacob H, Vives R, Vita C (2002) Heparin-aggregated RANTES can be crystallized. *Acta Crystallogr D* 58:1670–1673.
19. Rose GD, Fleming PJ, Banavar JR, Maritan A (2006) A backbone-based theory of protein folding. *Proc Natl Acad Sci USA* 103:16623–16633.
20. Dyson HJ, Wright PE (2005) Intrinsically unstructured proteins and their functions. *Nat Rev* 6:197–208.
21. Wright PE, Dyson HJ (1999) Intrinsically unstructured proteins: Reassessing the protein structure-function paradigm. *J Mol Biol* 293:321–331.
22. Wand AJ (2001) Dynamic activation of protein function: A view emerging from NMR spectroscopy. *Nat Struct Biol* 8:926–931.
23. Kern D, Zwietering ER (2003) The role of dynamics in allosteric regulation. *Curr Opin Struct Biol* 13:748–757.
24. Mittermaier A, Kay LE (2006) New tools provide new insights in NMR studies of protein dynamics. *Science* 312:224–228.
25. Shan L, et al. (2000) Identification of viral macrophage inflammatory protein (vMIP)-II as a ligand for GPR5/XCR1. *Biochem Biophys Res Commun* 268:938–941.
26. Mori S, Abeygunawardana C, Johnson MO, van Zijl PCM (1995) Improved sensitivity of HSQC spectra of exchanging protons at short interscan delays using a new fast HSQC (FHSQC) detection scheme that avoids water saturation. *J Magn Reson Ser B* 105: 94–98.
27. Grzesiek S, Bax A (1992) Improved 3D triple-resonance NMR techniques applied to a 31-kDa protein. *J Magn Reson* 96:432–440.
28. Kay LE, Xu GY, Yamazaki T (1994) Enhanced-sensitivity triple-resonance spectroscopy with minimal H<sub>2</sub>O saturation. *J Magn Reson Ser A* 109:129–133.
29. Muhandiram DR, Kay LE (1994) Gradient-enhanced triple-resonance three-dimensional NMR experiments with improved sensitivity. *J Magn Reson Ser B* 103:203–216.
30. Grzesiek S, Anglister J, Bax A (1993) Correlation of backbone amide and aliphatic side-chain resonances in <sup>13</sup>C/<sup>15</sup>N-enriched proteins by isotropic mixing of <sup>13</sup>C magnetization. *J Magn Reson Ser B* 101:114–119.
31. Kay LE, Xu G-Y, Singer AU, Muhandiram DR, Forman-Kay JD (1993) A gradient-enhanced HCCH-TOCSY experiment for recording side-chain <sup>1</sup>H and <sup>13</sup>C correlations in H<sub>2</sub>O samples of proteins. *J Magn Reson Ser B* 101:333–337.
32. Santoro J, King GC (1992) A constant-time 2D overbroadening experiment for inverse correlation of isotopically enriched species. *J Magn Reson* 97:202–207.
33. Delaglio F, et al. (1995) NMRPipe: A multidimensional spectral processing system based on UNIX pipes. *J Biomol NMR* 6:277–293.
34. Bartels C, Xia T-H, Billeter M, Güntert P, Wüthrich K (1995) The program XEASY for computer-supported NMR spectral analysis of biological macromolecules. *J Biomol NMR* 5:1–10.
35. Cornilescu G, Delaglio F, Bax A (1999) Protein backbone angle restraints from searching a database for chemical shift and sequence homology. *J Biomol NMR* 13:289–302.
36. Talluri S, Wagner G (1996) An optimized 3D NOESY-HSQC. *J Magn Reson B* 112:200–205.
37. Linge JP, Williams MA, Spronk CA, Bonvin AM, Nilges M (2003) Refinement of protein structures in explicit solvent. *Proteins* 50:496–506.
38. Schwieters CD, Kuszewski JJ, Tjandra N, Clore GM (2003) The Xplor-NIH NMR molecular structure determination package. *J Magn Reson* 160:65–73.
39. Farrow NA, Zhang O, Forman-Kay JD, Kay LE (1994) A heteronuclear correlation experiment for simultaneous determination of <sup>15</sup>N longitudinal decay and chemical exchange rates of systems in slow equilibrium. *J Biomol NMR* 4:727–734.